Discretization of the magnetic field in MPD thrusters

Jörg Heiermann and Monika Auweter-Kurtz
Institut für Raumfahrtsysteme, Universität Stuttgart, Stuttgart, Germany

Keywords *Plasma physics, Aerodynamics, Flow, Electromagnetic radiation*

Received February 2002
Revised November 2002
Accepted November 2002

Abstract *For the numerical simulation of magnetoplasmadynamic (MPD) self-field thruster flow, the solution of one of the two dynamical Maxwell equations – Faraday's law – is required. The Maxwell equations and Ohm's law for plasmas can be summarized in one equation for the stream function so that the two-dimensional, axisymmetric magnetic field can be calculated. The finite volume (FV) discretization of the equation on unstructured, adaptive meshes is presented in detail and solutions for different thruster currents are shown. The calculated thrust is compared with the experimental data.*

Introduction

Magnetoplasmadynamic (MPD) self-field thrusters are candidates for propelling manned spacecraft to Mars because they can achieve a high exhaust velocity combined with a high thrust density (Auweter-Kurtz, 1992; Bennett *et al.*, 1990; Jahn, 1968). The basic principle of self-field MPD propulsion is shown in Figure 1. Fuel is injected with a mass flow rate $\dot{m}$. It is heated and ionized by the electric discharge between anode and cathode so that a plasma is created. The plasma temperature can reach more than 40,000 K in the nozzle throat region. The electric current density $\vec{j}$ induces an azimuthal magnetic self-field $\vec{B}$ so that the plasma is accelerated by thermal expansion in the divergent nozzle as well as by the Lorentz force $\vec{j} \times \vec{B}$.

Since the early 1980s, MPD thrusters have been investigated at the Institut für Raumfahrtsysteme (IRS) experimentally, theoretically and numerically (Auweter-Kurtz *et al.*, 1998; Boie, 1999; Sleziona, 1998). Engineering aspects as well as basic plasma processes are considered in order to achieve higher efficiency and to avoid power-limiting plasma instabilities which are identified by voltage oscillations and increasing anode losses.

Numerical methods have been developed worldwide (Choueiri, 1999; Fujita, 1996; Minakuchi and Kuriki, 1984; Niewood and Martinez-Sanchez, 1991; Sankaran *et al.*, 2000; Turchi *et al.*, 1995) with the complexity of the discretized conservation equations increasing with the available computing power.

This work has been supported by the German Research Foundation DFG (Deutsche Forschungsgemeinschaft) through the project "Conservation Equations and Numerical Solutions for Technically Relevant Magneto-Plasmas" (Au 85/9-1,2,3), which belongs to the German Priority Research Program (Schwerpunktprogramm) "Analysis and Numerics for Conservation Laws".

International Journal of Numerical Methods for Heat & Fluid Flow
Vol. 14 No. 4, 2004
pp. 559-572

0961-5539
DOI 10.1108/09615530410532295

A new FV solver has been developed at the IRS for solving the conservation equations describing a continuum-mechanical, turbulent axisymmetric argon plasma flow under the influence of an arc discharge in thermal and reaction non-equilibrium (Heiermann and Auweter-Kurtz, 2001).

A novelty is the time-stabilized FV solution of the stream function which describes the distribution of the electric current on adaptive unstructured meshes. The formulation of the stream function equation and its discretization are explained in detail in the following sections.

Results are discussed for the thruster with hot anode HAT which has been built (Figure 2) and is being operated (Figure 3) at the IRS.

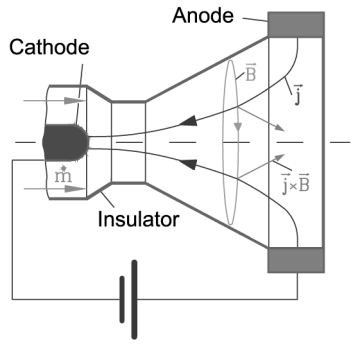

Figure 1.
Basic principle of self-field MPD propulsion

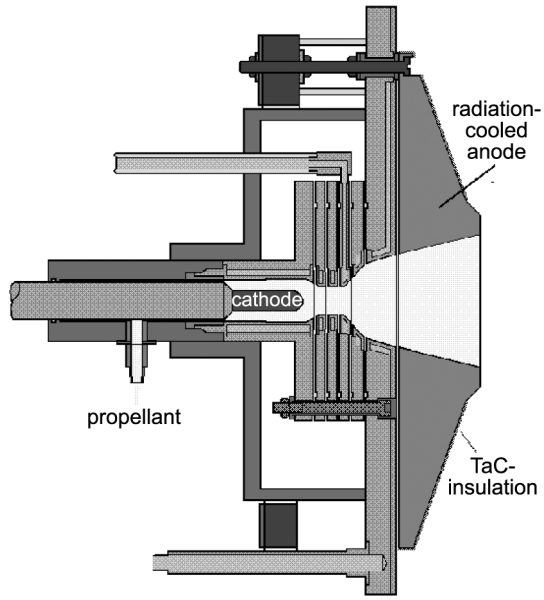

Figure 2.
The self-field MPD thruster with hot anode HAT

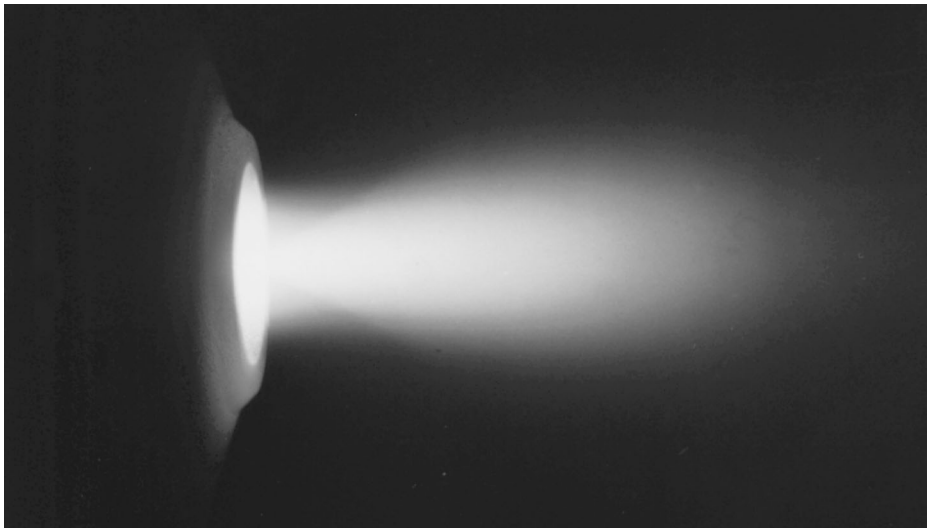

Figure 3.
HAT, firing, 2000 A, 0.8 g/s argon

Conservation equation for the magnetic field

For the derivation of the conservation equation for the magnetic field the Maxwell equations (Jackson, 1962) are required:

$$\text{rot}\,\vec{B} = \mu_0 \vec{j} + \frac{1}{c^2}\frac{\partial \vec{E}}{\partial t}, \tag{1}$$

$$\text{rot}\,\vec{E} = -\frac{\partial \vec{B}}{\partial t}, \tag{2}$$

$$\text{div}\,\vec{B} = 0 \tag{3}$$

and

$$\text{div}\,\vec{E} = \frac{\rho_{el}}{\varepsilon_0}. \tag{4}$$

Since a stationary solution shall be achieved and since no high frequency oscillations are considered, the Galilei-invariant formulation of equation (1) is used, neglecting the displacement current. Equation (3) is automatically fulfilled because of axisymmetry. In general, equation (4) can be used to calculate the charge density ρ_{el}. However, the plasmas considered can be assumed to be quasineutral so that ρ_{el} is zero.

Ohm's law for plasmas is given by (Cap, 1994)

$$\vec{E} = \frac{\vec{j}}{\sigma} - \vec{v} \times \vec{B} + \beta \vec{j} \times \vec{B} - \beta \nabla p_e. \tag{5}$$

It includes the electric conductivity σ (Devoto, 1973), the convection velocity $\vec{v}$ and the electron pressure p_e.

The Hall parameter

$$\beta = \frac{1}{en_e} \tag{6}$$

includes the electron density n_e.

The equations (1), (2) and (5) can be used to write the conservation equation for the magnetic field in cylindrical coordinates

$$\vec{B} = \begin{bmatrix} 0 \\ \mathrm{B} \\ 0 \end{bmatrix} \tag{7}$$

with the azimuthal component B:

$$\frac{\partial B}{\partial t} = -\mathrm{div}(B\vec{v}) + \frac{Bv_r}{r} - \mathrm{rot}\left(\frac{\mathrm{rot}\,\vec{B}}{\mu_0\sigma} + \frac{\beta}{\mu_0}\mathrm{rot}\,\vec{B}\times\vec{B} - \beta\nabla p_e\right)_\varphi . \tag{8}$$

The first term on the right hand side describes the convective transport of the magnetic field, the second term appears because of the use of cylindrical coordinates. The third term describes the change of the magnetic field by the electric current density $\vec{j}$ by the Hall current and by the ∇p_e term. Finally, the magnetic field B in equation (8) can be substituted by the stream function

$$\Psi = rB \tag{9}$$

and subsequently, the conservation equation for the magnetic field becomes

$$\frac{1}{r}\frac{\partial \Psi}{\partial t} = -\mathrm{div}\left(\frac{\Psi}{r}\vec{v}\right) + \frac{\Psi v_r}{r^2} - \mathrm{rot}\left(\frac{1}{\mu_0\sigma}\mathrm{rot}\begin{bmatrix} 0 \\ \Psi/r \\ 0 \end{bmatrix} + \frac{\beta}{\mu_0}\mathrm{rot}\begin{bmatrix} 0 \\ \Psi/r \\ 0 \end{bmatrix} \times \begin{bmatrix} 0 \\ \Psi/r \\ 0 \end{bmatrix} - \beta\nabla p_e\right). \tag{10}$$

This equation shall be iterated until a steady-state solution for the stream function is achieved. The contour lines of the stream function represent the stream lines of the electrons which carry the electric current. Hence, a constant electric current flows between two neighboring contour lines of the stream function.

The boundary condition on the eletrodes is that the electric field vector only has a component perpendicular to the electrode surfaces. Ampére's law is applied everywhere else as Dirichlet condition for Ψ:

$$\Psi = \frac{\mu_0 I}{2\pi}, \tag{11}$$

where I is the thruster current.

Discretization

Owing to the complex geometry of MPD thrusters, the spatial discretization is done on unstructured meshes. Appropriate adaptation (Iben *et al.*, 2000) of coarse initial meshes reduces the amount of computational time significantly. An advancing front algorithm is used to create a primary triangulation of the computational domain. The geometric centers of mass of the triangles are connected to create the so-called dual cells, see Figure 4. The connection of the centers of mass $\vec{x}_m$ of the dual cells creates the so-called "dual triangles". The dual triangles are the result of the choice of cylindrical coordinates; the centers of mass of the dual cells are not the geometric centers of mass.

A toroidal cell face is defined by its area ΔA_{ik}, the normal unit vector $\vec{n}_{ik}$ and the Gauß point $\vec{x}_{ik}$. Additionally, the dual triangles $\mathcal{T}_{ijk}$ and $\mathcal{T}_{ikl}$ and the physical states left (l) and right (r) of the cell face are attached to the cell face.

For the discretization of equation (10) the theorems of Gauß

$$\int_{\Delta V_\omega} \operatorname{div} \vec{a}\, \mathrm{d}\Delta V_\omega = \int_{\Delta A_{\omega k}} \vec{a}\, \mathrm{d}\Delta \vec{A}_{\omega k} \tag{12}$$

and Stokes

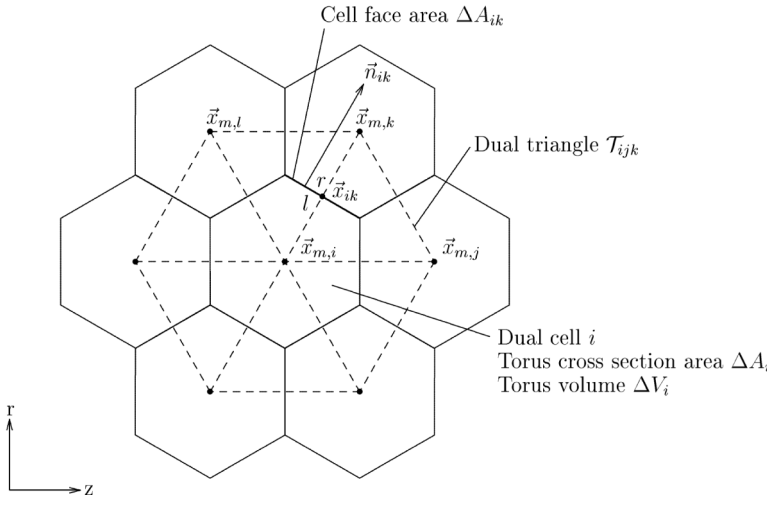

Figure 4.
Dual cells as control volumes

$$\int_{\Delta A_\omega} \mathrm{rot}\,\vec{E}\,\mathrm{d}\Delta\vec{A}_\omega = \oint_{\partial\omega} \vec{E}\,\mathrm{d}\vec{l}_{\partial\omega} \tag{13}$$

are needed on each dual cell ω.

The theorem of Gauß is applied to the convective part, and the theorem of Stokes to the rest of the right hand side of equation (10). The discretized right hand side is written as:

$$\begin{aligned}\mathrm{RHS}^B = &-\frac{1}{\Delta V_\omega}\sum_{k=1}^{K} F^B_{WENO}(\vec{x}_{\omega k})\Delta A_{\omega k} + \frac{\frac{\Psi}{r_{m,\omega}}v_r}{\left(\frac{1}{K+1}\sum_{\substack{k=1\\k=\omega}}^{K} r^3_{m,k}\right)^{1/3}} \\ &-\frac{1}{\Delta A_\omega}\sum_{k=1}^{K}\frac{1}{2}\left[\frac{(\mathrm{rot}\,\vec{B})_{\mathcal{T}_{\omega jk}}}{\mu_0\overline{\sigma_{\omega jk}}} + \frac{(\mathrm{rot}\,\vec{B})_{\mathcal{T}_{\omega kl}}}{\mu_0\overline{\sigma_{\omega kl}}} + \frac{\overline{\beta_{\omega jk}}}{\mu_0}(\mathrm{rot}\,\vec{B})_{\mathcal{T}_{\omega jk}} \times \overline{\vec{B}_{\omega jk}}\right. \\ &\left. + \frac{\overline{\beta_{\omega kl}}}{\mu_0}(\mathrm{rot}\,\vec{\beta})_{\mathcal{T}_{\omega kl}} \times \overline{\vec{B}_{\omega kl}} - \overline{\beta_{\omega jk}}(\nabla p_\mathrm{e})_{\mathcal{T}_{\omega jk}} - \overline{\beta_{\omega kl}}(\nabla p_\mathrm{e})_{\mathcal{T}_{\omega kl}}\right]\left[\overline{\vec{x}_{\omega kl}} - \overline{\vec{x}_{\omega jk}}\right].\end{aligned} \tag{14}$$

$\mathrm{F}^B_{\mathrm{WENO}}(\vec{x}_{\omega k})$ denotes the convective flux of the magnetic field for which the variables have been linearly reconstructed on each dual cell by a weighted essentially non-oscillatory (WENO) scheme (Friedrich, 1998). The WENO scheme assures second-order accuracy of the spatial solution.

The flux $\mathrm{F}^B_{\mathrm{WENO}}(\vec{x}_{\omega k})$ at the Gauß point $\vec{x}_{\omega k}$ is computed with a flux vector splitting scheme. The magnetoacoustic speed is defined as

$$\mathrm{c} = \sqrt{\frac{\gamma(p_\mathrm{h} + p_\mathrm{e})}{\rho} + \frac{B^2}{\mu_0\rho}}. \tag{15}$$

One now defines a new reference speed

$$\mathrm{s} = \sqrt{\alpha c^2 + q^2\left(1 - 2\alpha + \alpha\frac{q^2}{c^2}\right)}, \tag{16}$$

with

$$q^2 = \min\left(c^2, \mathrm{q}_n^2\right). \tag{17}$$

α is chosen as

$$\alpha = \frac{2}{\gamma\phi} \tag{18}$$

with $\gamma = 5/3$ being the adiabatic coefficient. The velocity normal to the cell face of two neighbouring dual cells is

$$q_n = v_z n_z + v_r n_r. \tag{19}$$

The eigenvalues are defined as

$$\begin{aligned} \lambda_0 &= q_n, \\ \lambda_1 &= \lambda_0 + s, \\ \lambda_2 &= \lambda_0 - s. \end{aligned} \tag{20}$$

With the physical states left (l) and right (r) of a cell face the following equations are chosen for the splitting:

$$h_{1l} = \frac{1}{4}(\lambda_{1l} + |\lambda_{1l}|), \tag{21}$$

$$h_{1r} = \frac{1}{4}(\lambda_{1r} - |\lambda_{1r}|), \tag{22}$$

$$h_{2l} = \frac{1}{4}(\lambda_{2l} + |\lambda_{2l}|), \tag{23}$$

$$h_{2r} = \frac{1}{4}(\lambda_{2r} - |\lambda_{2r}|). \tag{24}$$

The upwind flux function for the magnetic field is

$$F^B = B_l(h_{1l} + h_{2l}) + B_r(h_{1r} + h_{2r}). \tag{25}$$

In the source term in equation (10) an averaged radius is used to preserve symmetry in the discrete case. Overlined values represent average values on a dual triangle.

The remaining parts of equation (10) are discretized in a central manner. The distances

$$\left[\overline{\vec{x}_{\omega kl}} - \overline{\vec{x}_{\omega jk}}\right]$$

represent the border of the toroidal cross section ΔA_ω of a dual cell ω. The average values $\overline{\vec{x}_{\omega kl}}$ and $\overline{\vec{x}_{\omega jk}}$ are calculated on the primary triangles and represent the corners of a dual cell ω.

The current density $\vec{j}$ is calculated by

$$(\mathrm{rot}\,\vec{B})_{\mathcal{T}_{\omega jk}} = \mu_0 \begin{bmatrix} j_z \\ [0.5ex] \\ j_r \end{bmatrix}_{\mathcal{T}_{\omega jk}} = \mu_0 \begin{bmatrix} \dfrac{1}{\overline{\overline{r_{m,\omega jk}}}} \left(\dfrac{\partial \Psi}{\partial r}\right)_{\mathcal{T}_{\omega jk}} \\ [0.5ex] \\ -\dfrac{1}{\overline{\overline{r_{m,\omega jk}}}} \left(\dfrac{\partial \Psi}{\partial z}\right)_{\mathcal{T}_{\omega jk}} \end{bmatrix}. \tag{26}$$

Since a steady-state solution is required, an explicit first-order time stepping scheme is employed for time-stabilization. The calculation of the explicit local time step for equation (10) considers the magnetic diffusion which is in some sense comparable with a classical heat conduction problem. All K neighbouring cells are included:

$$\Delta t_B = \mathrm{CFL}_B \frac{\mu_0}{2} \frac{1}{K+1} \sum_{\substack{k=1 \\ k=\omega}}^{K} \sigma_k \left(\frac{1}{K} \sum_{k=1}^{K} |\vec{x}_{m,k} - \vec{x}_{m,\omega}| \right)^2. \tag{27}$$

The CFL_B number dampens the other mechanisms in Ohm's law, which are not considered in equation (27).

Before the actual time stepping is performed, all local time steps are multiplied with different random numbers RND between 0 and 1:

$$\Delta t_{B,\mathrm{RND}} = \Delta t_B \mathrm{RND}_B. \tag{28}$$

The time integration for the stream function Ψ

$$\Psi^{n+1} - \Psi^n = \Delta t_{B,\mathrm{RND}} \left[\left(1 - \frac{1}{K}\right) \mathrm{RHS}_{\omega}^{B} r_{m,\omega} + \frac{1}{K} \frac{\sum_{k=1}^{K} \mathrm{RHS}_{k}^{B} r_{m,k}}{K} \right]. \tag{29}$$

includes local residual smoothing.

The requirement of robustness is the reason for the choice of first-order time-stepping. Higher-order schemes like Runge-Kutta schemes generally accelerate convergence as long as the right hand sides are relatively simple. In the case of the complex non-linear right hand side presented here, they tend to produce numerical oscillations.

The random time stepping also adds stability. It allows an increase of the CFL_B number by about an order of magnitude. Although its mathematical properties are not yet understood, it is clear that it introduces a non-linear, dampening dissipation which disappears once the steady-state solution is

achieved. It should be mentioned here that the results obtained with and without random time steps are similar.

Results

A typical discretization of the computational domain is shown in Figure 5. In the nozzle area, the mesh is highly refined for a good resolution of the boundary layers and for capturing the oblique shock (Figures 6 and 7) which is visible during the experiment when the HAT is being fired in one of the test chambers in the IRS laboratory (Figure 3).

While the shock is clearly visible in the heavy particle temperature T_h, it cannot be seen in the current distribution (Figure 8). Obviously, the convective

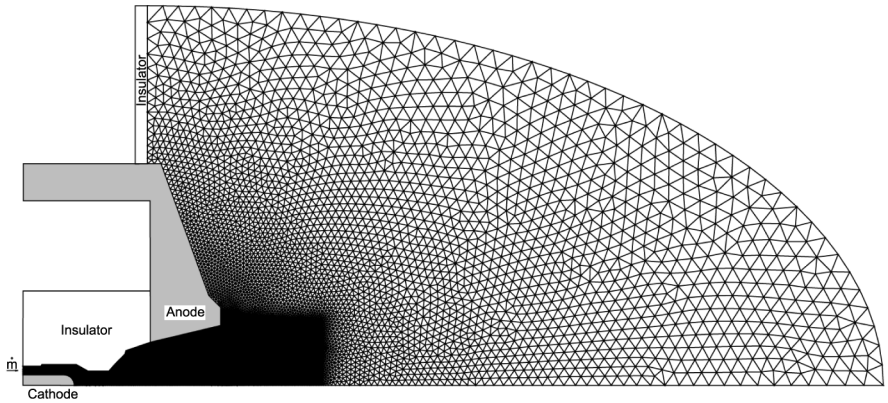

Figure 5.
HAT, entire adapted mesh with 28,034 cells, 2,000 A, 0.8 g/s argon

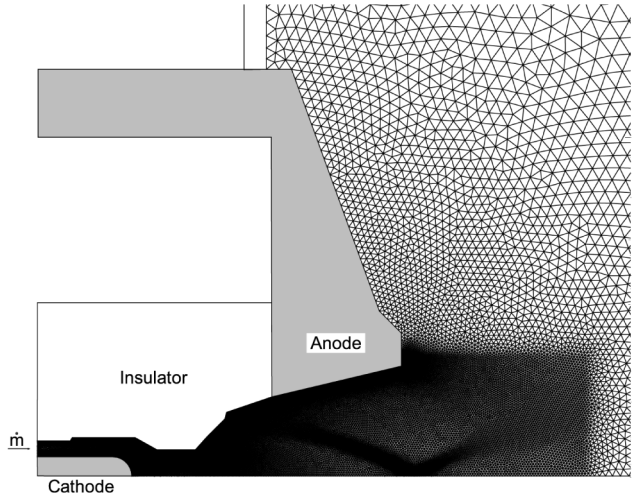

Figure 6.
HAT, adapted mesh with highly resolved boundary layers and oblique shock, 2,000 A, 0.8 g/s argon

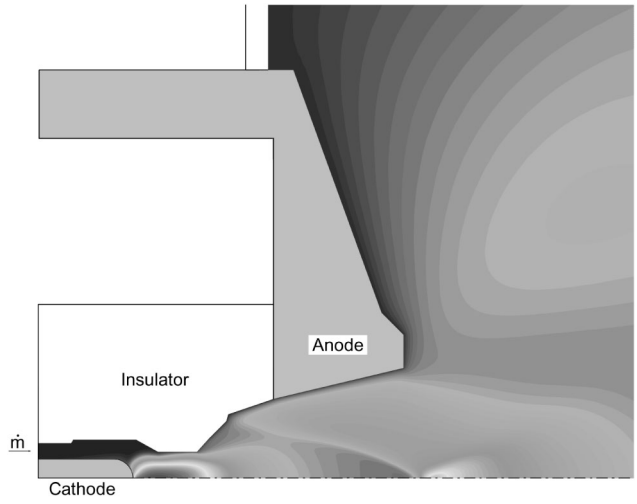

Figure 7.
HAT, heavy particle temperature, 2,000 A, 0.8 g/s argon

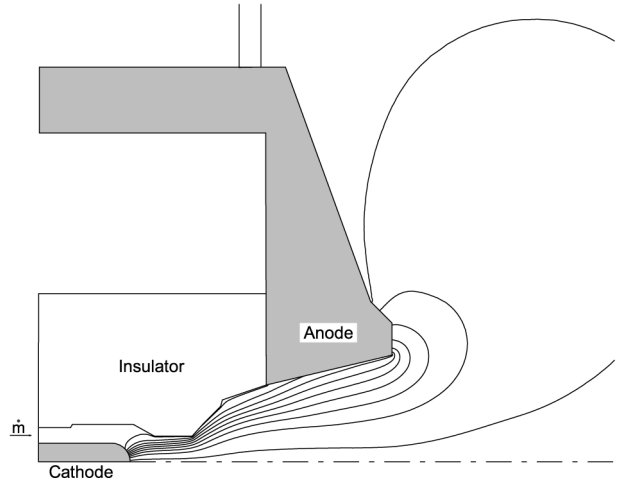

Figure 8.
HAT, stream function Ψ (250 A between two isolines), 2,000 A, 0.8 g/s argon

term in equation (10) is dominated by the other terms and the physical mechanisms they represent.

The evolution of the current distribution with increasing thruster current (Figures 8-11) shows that, beginning at about 4,000 A, the electric arc starts to constrict downstream of the nozzle throat because of the pinch effect.

Also, the arc attachment on the anode surface varies strongly with changing thruster current. The detailed analysis of the plasma/electrode interaction (Goodfellow, 1996; Hügel, 1980) is part of the current work at the IRS. The distribution of Ψ is mostly smooth, and slight oscillations only appear for

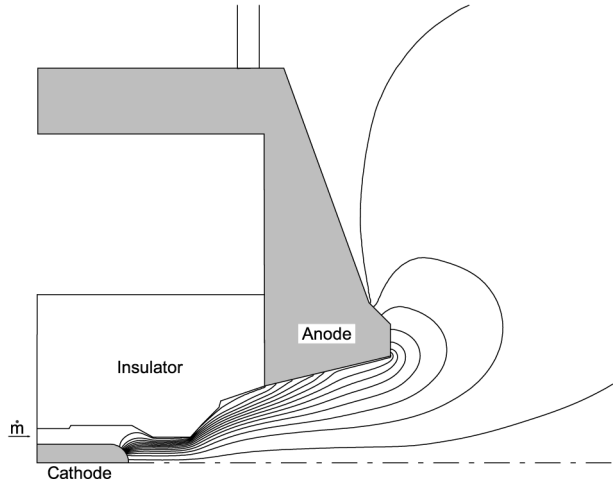

Figure 9.
HAT, stream function Ψ (250 A between two isolines), 3,000 A, 0.8 g/s argon

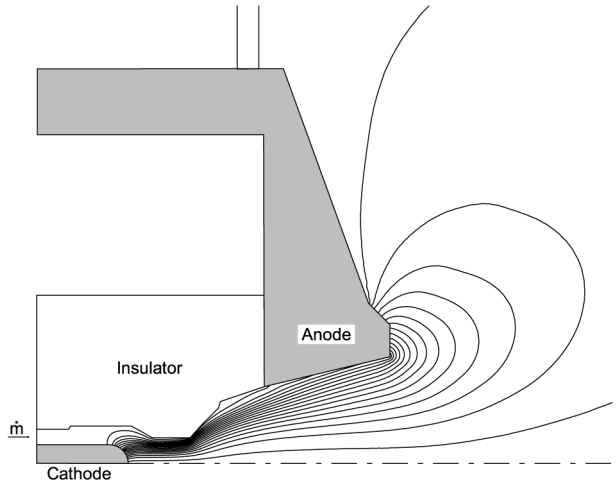

Figure 10.
HAT, stream function Ψ (250 A between two isolines), 4,000 A, 0.8 g/s argon

5,000 A where the pinch effect reduces the particle density downstream of the nozzle throat drastically.

The discretization is very robust and efficient. The results for Ψ deliver source terms in the conservation equations which are not discussed here. For example, the Lorentz force acceleration of the heavy particles and the Ohmic heating of the electron gas require smooth solutions of Ψ which is guaranteed by the discretization presented here.

The thrust can be calculated in the anode cross section as

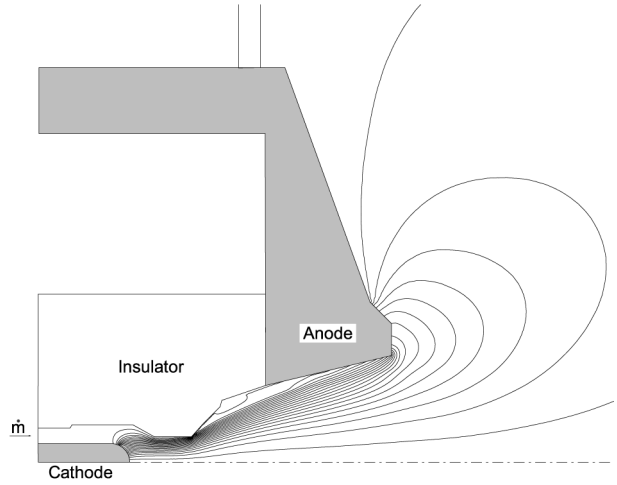

Figure 11.
HAT, stream function Ψ (250 A between two isolines), 5,000 A, 0.8 g/s argon

$$F = \sum_{\Delta A} \left(p_{\mathrm{h}} + p_{\mathrm{e}} + \frac{B^2}{2\mu_0} + \rho v_z^2 \right) \Delta A. \tag{30}$$

Results are given in Table I. The thruster is mounted on a thrust measurement stand in the test chamber to measure the thrust force. Since the thrust stand is being thermally heated in a non-uniform way during the thruster firings, the experimentally measured thrust data show some drifting. However, there is a good agreement between numerical and experimental data. A further evaluation of numerical and experimental results will be possible when electrode phenomena are included so that, for example, the voltage can be compared.

Conclusion

A new FV discretization for the conservation equation of the magnetic field in self-field MPD thrusters has been developed for unstructured adaptive meshes. Proper second-order upwinding and central discretization and explicit first-order stepping including randomization and residual smoothing deliver smooth steady-state solutions in a quick and robust way.

Table I.
Thrust data for the HAT (num.: numerical, exp.: experimental)

I(A)	$\dot{m}$ (g/s)	F(N) num.	F(N) exp.
2,000	0.8	4.3	3.7-4.7
3,000	0.8	5.9	5.7-7.0
4,000	0.8	8.5	7.8-9.4
5,000	0.8	10.1	11.1

Numerical and experimental data for the thrust agree well. In the next step, the plasma/electrode interaction will be investigated.

References

Auweter-Kurtz, M. (1992), *Lichtbogenantriebe für Weltraumaufgaben*, B.G. Teubner, Stuttgart.

Auweter-Kurtz, M., Boie, C., Habiger, H., Kaeppeler, H.J., Kurtz, H.L., Sleziona, P.C., Wegmann, T. and Winter, M.W. (1998), "Numerische Simulation von MPD–Triebwerken und Vergleich mit durchzuführenden experimentellen Untersuchungen", Universität Stuttgart, Stuttgart, Final Report of the DFG project Au85/5-2, Institut für Raumfahrtsysteme.

Bennett, G.L., Watkins, M.A., Byers, D.C. and Barnett, J.W. (1990), "Enhancing space transportation: the NASA program to develop electric propulsion", *IEPC-91-004, 21st AIAA/DGLR/JSASS International Electric Propulsion Conference*, Orlando, FL.

Boie, C. (1999), "Numerische Simulation magnetoplasmadynamischer Eigenfeldtriebwerke mit hochauflösenden adaptiven Verfahren", PhD thesis, Institut für Raumfahrtsysteme, Fakultät Luft- und Raumfahrttechnik, Universität Stuttgart, Stuttgart.

Cap, F. (1994), *Lehrbuch der Plasmaphysik und Magnetohydrodynamik*, Springer, Wien, NY.

Choueiri, E.Y. (1999), "Anomalous resistivity and heating in current-driven plasma thrusters", *Physics of Plasmas*, Vol. 6 No. 5, pp. 2290-306.

Devoto, R.S. (1973), "Transport coefficients of ionized argon", *The Physics of Fluids*, Vol. 16 No. 5, pp. 616-23.

Friedrich, O. (1998), "Weighted essentially non-oscillatory schemes for the interpolation of mean values on unstructured grids", *Journal of Computational Physics*, Vol. 144, pp. 194-212.

Fujita, K. (1996), "Performance computation of a low-power hydrogen arcjet", *AIAA-96-3183, 32nd Joint Propulsion Conference*, Lake Buena Vista, FL.

Goodfellow, K.D. (1996), "A theoretical and experimental investigation of cathode processes in electric thrusters", PhD thesis, Faculty of the Graduate School, University of Southern California, CA.

Heiermann, J. and Auweter-Kurtz, M. (2001), "Numerical simulation of high power steady state MPD thrusters", *IEPC-01-128, 27th International Electric Propulsion Conference*, Pasadena, CA.

Hügel, H. (1980), "Zur Funktionsweise der Anode im Eigenfeldbeschleuniger", Habilitation thesis, Fakultät Luft- und Raumfahrttechnik, Universität Stuttgart, DFVLR Research Report, 80-20 Stuttgart.

Iben, U., Warnecke, G., Heiermann, J. and Auweter-Kurtz, M. (2000), "Adaptive numerics for the simulation of magneto-plasmadynamic rocket thrusters", in Neittaanmäki, P., Tiihonen, T. and Tarvainen, P. (Eds), *Proceedings of The Third European Conference on Numerical Mathematics and Advanced Applications*, World Scientific, Singapore, Jyväskylä, Finland, pp. 121-30.

Jackson, J.D. (1962), *Classical Electrodynamics*, Wiley, New York, NY.

Jahn, R.G. (1968), *Physics of Electric Propulsion*, McGraw-Hill Series in Missile and Space Technology, USA.

Minakuchi, H. and Kuriki, K. (1984), "Magnetoplasmadynamic analysis of plasma acceleration", *AIAA-84-06, Proceedings of the 17th International Electric Propulsion Conference*, Tokyo, Japan.

Niewood, E.H. and Martinez-Sanchez, M. (1991), "A two-dimensional model of an MPD thruster", *AIAA 91-2344, 27th AIAA/SAE/ASME Joint Propulsion Conference*, Sacramento, CA.

Sankaran, K., Choueiri, E.Y. and Jardin, S.C. (2000), "Application of a new numerical solver to the simulation of MPD flows", *AIAA-2000-3537, 36th AIAA/ASME/SAE/ASEE Joint Propulsion Conference*, Huntsville, AL.

Sleziona, P.C. (1998), "Hochenthalpieströmungen für Raumfahrtanwendungen", Habilitation thesis, Fakultät Luft- und Raumfahrttechnik, Universität Stuttgart, Stuttgart.

Turchi, P.J., Mikellides, P.G., Hohman, K.W., Leiweke, R.J., Mikellides, I.G., Schmahl, C.S., Roderick, N.F. and Peterkin, R.E. Jr (1995), "Progress in modeling plasma thrusters and related plasma flows", *IEPC-95-159, Proceedings of the 24th International Electric Propulsion Conference*, Moscow, Russia.